Journal of Computational Physics 259 (2014) 96–113

Contents lists available at ScienceDirect

Journal of Computational Physics

www.elsevier.com/locate/jcp

Unified gas-kinetic scheme for diatomic molecular simulations in all flow regimes

Sha Liu [a], Pubing Yu [b], Kun Xu [b,*], Chengwen Zhong [a]

[a] National Key Laboratory of Science and Technology on Aerodynamic Design and Research, Northwestern Polytechnical University, Xi'an, Shaanxi 710072, China
[b] Mathematics Department, Hong Kong University of Science and Technology, Clear Water Bay, Kowloon, Hong Kong

ARTICLE INFO

Article history:
Received 21 July 2013
Received in revised form 17 October 2013
Accepted 27 November 2013
Available online 1 December 2013

Keywords:
Unified gas-kinetic scheme
Diatomic molecules
Rarefied flows
Hypersonic non-equilibrium flows

ABSTRACT

A unified gas-kinetic scheme (UGKS) is constructed for both continuum and rarefied flow computations. The underlying principle for the development of UGKS is the direct modeling for the gas evolution process from the kinetic to the hydrodynamic scale, which is used in the flux construction across a cell interface. More specifically, the physical process from the kinetic particle free transport to the hydrodynamic pressure wave propagation is recovered in the flux function. In the previous study, the UGKS has been developed mainly for monatomic gas with particle translational motion only. The construction of time evolution solution is based on the BGK, Shakhov, and ES–BGK models. The UGKS has been validated through extensive numerical tests. In this paper, a UGKS for diatomic gas will be constructed, where the gas-kinetic Rykov model with a Landau–Teller–Jeans-type rotational energy relaxation is used in the numerical scheme. The new scheme will be tested in many cases, such as homogeneous flow relaxation, shock structure calculations, hypersonic flow passing a flat plate, and the flow around a blunt circular cylinder. The analytic, DSMC, and experimental measurements will be used for validating the solutions of UGKS.

1. Introduction

The flow regime is categorized according to the Knudsen number Kn, which is a defined as the ratio of the molecular mean free path to a characteristic physical length scale. The value of the Knudsen number determines the validity of different approaches in the description of gas flow, such as the hydrodynamic method or statistical one. The whole flow regime is qualitatively divided into continuum ($Kn < 0.01$), transitional ($0.01 < Kn < 10$), and free molecular regimes ($Kn > 10$).

In many scientific and engineering applications, such as space exploration, vacuum technology, micro-electro-mechanical systems development, both continuum and rarefied flow regimes can be encountered in a single case of flow study. In order to correctly capture such a crossing scale solution, the development of a unified scheme becomes necessary. By modeling the time evolution of a gas distribution function due to the free transport and binary elastic collision, the Boltzmann equation has been constructed for monatomic dilute gas. The modeling scale of the Boltzmann equation is the particle mean free path and mean collision time. Theoretically, kinetic schemes can be developed by direct discretization of the Boltzmann equation for all flow regimes if the numerical cell size and time step used are consistent with the modeling scale of the kinetic equation, such as mean free path and particle collision time. But, this approach is purely a brutal force method which can be hardly used in real engineering applications for the flow close to the continuum regime. The development

* Corresponding author.
E-mail addresses: shaliu@mail.nwpu.edu.cn (S. Liu), mayupb@ust.hk (P. Yu), makxu@ust.hk (K. Xu), zhongcw@nwpu.edu.cn (C. Zhong).

0021-9991/$ – see front matter
http://dx.doi.org/10.1016/j.jcp.2013.11.030

of a unified scheme for all flow regimes is somehow more difficult than the construction of kinetic equation with a single modeling scale, such as the Boltzmann equation.

Currently, based on the kinetic equation there are two kinds of numerical methods for simulating non-equilibrium dilute gases, i.e., statistical and deterministic ones. The statistical method, represented by the Direct Simulation Monte Carlo (DSMC) method [1–3], uses probabilistic simulation to solve the Boltzmann equation. The deterministic method, such as the Discrete Velocity Methods (DVM) or Discrete Ordinate Method (DOM) [4–9], use regular numerical discretization of particle velocity space to solve the Boltzmann equation. Besides the above approaches, many other methods, such as the finite difference [10], spectral [11,12], and multi-scale lattice Boltzmann methods [13], have been developed as well. In order to simplify the numerical schemes for the Boltzmann equation, both statistical and deterministic methods use an operator splitting approach, such as decoupling the transport and collision process into a collisionless free transport and particle collision. In order to validate such an operator splitting method, such as avoiding introducing numerical error due to splitting, the cell size and time step in these numerical schemes are limited by the particle mean free path and mean collision time. Therefore, these methods are capable of simulating high Knudsen number flow efficiently. However, in the transition and continuum flow regimes, due to intensive particle collisions, the constraint on the cell size and time step makes operator splitting method be prohibitively expensive. Many studies have been concentrated on the development of asymptotic preserving schemes with implicit or semi-implicit treatments [9,14,15]. Based on the DVM approach, many kinetic solvers have been developed for diatomic gases as well [16–19]. For the lattice Boltzmann method (LBM), in order to get hydrodynamic solution it seems that the constraint of time step being less than the particle collision time is not needed [13]. The reason for LBM is that it solves the incompressible flow equations in the continuum limit, where the operator splitting error can be luckily absorbed into the physical viscous term by changing the viscosity coefficient.

In recent study, a unified gas-kinetic scheme (UGKS) based on the kinetic BGK and Shakhov models has been developed for monatomic gas for the whole flow regimes [20–24]. The unified scheme is a multi-scale method with coupled particle transport and collision in its numerical flux modeling. An integral solution of the gas-kinetic model has been used to construct the flow evolution around a cell interface. This time evolution solution covers the flow physics from the kinetic scale particle free transport to the hydrodynamic scale wave propagation, and the weight between these two limiting solutions depends on the ratio of time step to the local particle collision time. As a result, both kinetic and hydrodynamic solutions can be automatically obtained in the unified approach. Due to the un-splitting treatment for the transport and collision in UGKS, the time step used is not limited by the particle collision time. Therefore, the UGKS is more efficient than DVM and DSMC methods in the low transition and continuum flow computations. Even though the UGKS has been developed for the kinetic model equations, it provides a general framework to construct multi-scale method, such as the extension to the radiative transfer [25]. Even for the full Boltzmann equation, the corresponding scheme can be developed as well.

More specifically, the main difference between the UGKS and many other kinetic equation solvers is the flux evaluation across a cell interface. In UGKS [20], the time dependent flux function is obtained from a time evolution gas distribution function. As an illustration of the basic idea, a simplified version of the distribution function for the flux evaluation can be written as

$$f(t) = \eta(\Delta t/\tau) f_{NS} + \big(1 - \eta(\Delta t/\tau)\big) f_{free\text{-}transport},$$

where the parameter η depends on the ratio of time step Δt to the particle collision time τ, f_{NS} is the distribution function corresponding to the Navier–Stokes solution, and $f_{free\text{-}transport}$ presents the collisionless solution. Therefore, in both free molecular ($\Delta t \ll \tau$) and continuum ($\Delta t \gg \tau$) limits, the UGKS presents the exact solutions. In the transition regime ($\Delta t \sim \tau$), the UGKS has been validated extensively through numerical tests and the comparison with DSMC solutions. However, for most other kinetic equation solvers, the free transport $f_{free\text{-}transport}$ is solely used to model the interface flux, which corresponds to the flux vector splitting (FVS) scheme in the continuum limit. As a result, the dissipation in FVS is always proportional to the time step Δt instead of the physical collision time τ, and $\Delta t \gg \tau$ in the continuum limit deteriorates the accuracy of these schemes. So, we believe that it will be extremely hard for many kinetic solvers, which target for the rarefied flows, to pass the test case in the continuum flow regime [26]. The UGKS methodology has been adapted in the discrete unified gas-kinetic scheme (DUGKS) [27], which has extended the validity of the Lattice Boltzmann Method (LBM) from continuum to the rarefied regimes. The UGKS updates both gas distribution function and macroscopic flow variables. In the continuum flow regime, the Navier–Stokes equations are the well-defined governing equations and it becomes unnecessary to update the distribution function anymore. Actually, the distribution function in the continuum regime can be directly reconstructed from macroscopic flow variables and can be used for the flux evaluation in finite volume NS flow solver [28]. Therefore, even with the same accuracy in the continuum flow regime, the gas-kinetic scheme (GKS) for NS is much more efficient than UGKS.

The early UGKS has been constructed for monatomic gas. This paper concerns the extension of the UGKS to diatomic gas. In the diatomic gas modeling, the rotational degree of freedom is included and modeled by controlling the energy exchange between translational and rotational energy through the relaxation model. More specifically, the Rykov kinetic model is used to construct the time evolution solution of a gas distribution function [29].

This paper is organized in the following. The unified scheme will be presented in Section 2. Section 3 is the analysis of the scheme. Section 4 includes many numerical test cases to validate the proposed method. The last section is the discussion and concluding remarks.

2. Unified gas-kinetic scheme for diatomic molecules

2.1. Gas-kinetic models

For diatomic gas, besides the translational degrees of freedom, the internal degrees of freedom have to be included as well in a gas distribution function, i.e., $f(t,\mathbf{x},\mathbf{u},\epsilon)$, where the internal energy ϵ is $\epsilon = M^2/2J$ with moment of inertia J and angular momentum $\mathbf{M}$. The relations between distribution function and macro-variables are defined as

$$\begin{aligned}
\rho &= mn = \int mf\,du\,dv\,dw\,d\epsilon,\\
U_i &= \frac{1}{n}\int u_i f\,du\,dv\,dw\,d\epsilon,\\
P_{ij} &= \int mc_i c_j f\,du\,dv\,dw\,d\epsilon,\\
P_{tran} &= nkT_{tran} = \frac{1}{3}\int mc^2 f\,du\,dv\,dw\,d\epsilon,\\
P_{rot} &= nkT_{rot} = \int \epsilon f\,du\,dv\,dw\,d\epsilon,\\
q_{tran,i} &= \int c_i\frac{mc^2}{2} f\,du\,dv\,dw\,d\epsilon,\\
q_{rot,i} &= \int c_i\epsilon f\,du\,dv\,dw\,d\epsilon,
\end{aligned} \tag{1}$$

where $\mathbf{c} = (u-U, v-V, w-W)$ is the peculiar velocity, n is the particle number density, U_i is the i-direction flow velocity, T_{tran} is the translational temperature, T_{rot} is the rotational temperature, $q_{tran,i}$ is the heat flux related to translational degrees of freedom, and $q_{rot,i}$ is the heat flux due to the rotational energy transport.

In order to simplify the collisional model of the full Boltzmann equation, many kinetic models have been proposed and used in the study of rarefied flows [30–35]. For modeling diatomic gases, the non-equilibrium rotational and transitional energy should be considered. Many attempts have been done to construct kinetic models and develop the corresponding gas-kinetic schemes [36–39].

In this paper, the Rykov model [29] for diatomic gas will be used in the construction of UGKS. The Rykov model is an extension of the Shakhov model of monatomic gas. The Rykov model has the following form,

$$\frac{\partial f}{\partial t} + u\frac{\partial f}{\partial x} + v\frac{\partial f}{\partial y} + w\frac{\partial f}{\partial z} = \frac{g_{tran}-f}{\tau} + \frac{g_{rot}-g_{tran}}{Zr\tau}, \tag{2}$$

where the collision operator on the right-hand of the equation is consisted of two terms corresponding to the elastic and inelastic collisions respectively. The translational kinetic energy is conserved in the elastic collisions, while, in the inelastic collisions, the energy exchange between the translational and rotational energy takes place. In Eq. (2), g_{tran} is the equilibrium state in the elastic collisions and g_{rot} is the equilibrium state for inelastic collisions with the consideration of energy exchange and total energy conservation. The equilibrium states are expressed as

$$\begin{aligned}
g_{tran} &= n\left(\frac{m}{2\pi kT_{tran}}\right)^{\frac{3}{2}} e^{-\frac{mc^2}{2kT_{tran}}}\left(\frac{1}{kT_{rot}}\right)e^{-\frac{\epsilon}{kT_{rot}}}\left[1-\frac{2m\mathbf{q}_{tran}\cdot\mathbf{c}}{15kT_{tran}p_{tran}}\left(\frac{5}{2}-\frac{mc^2}{2kT_{tran}}\right)+(\sigma-1)\frac{m\mathbf{q}_{rot}\cdot\mathbf{c}}{kT_{tran}}\frac{kT_{rot}-\epsilon}{\theta}\right],\\
g_{rot} &= n\left(\frac{m}{2\pi kT}\right)^{\frac{3}{2}} e^{-\frac{mc^2}{2kT}}\left(\frac{1}{kT}\right)e^{-\frac{\epsilon}{kT}}\left[1-\omega_0\frac{2m\mathbf{q}_{tran}\cdot\mathbf{c}}{15kTp}\left(\frac{5}{2}-\frac{mc^2}{2kT}\right)+\omega_1\frac{m\mathbf{q}_{rot}\cdot\mathbf{c}}{kTp}\left(1-\frac{\epsilon}{kT}\right)\right],
\end{aligned} \tag{3}$$

where $\tau = \mu(T_{tran})/P_{tran} = \mu(T_{tran})/nkT_{tran}$ is the mean collision time, $1/\tau$ is the mean collision frequency, $\mu(T_{tran})$ is the viscosity of a diatomic gas, and T is the equilibrium temperature for translational and rotational degrees of freedom. The mean collision time τ depends on translational temperature T_{tran}, because the translational temperature characterizes the mean relative velocity of colliding particles. Here Zr is the rotation collision number which is related to the ratio of elastic collision frequency to inelastic frequency. And θ and σ are defined by

$$\begin{aligned}
\theta &= \int (kT_{rot}-\epsilon)^2 f\,du\,dv\,dw\,d\epsilon,\\
\sigma &= \frac{\mu(T_{tran})}{mnD},
\end{aligned} \tag{4}$$

where D is the self-diffusion of the diatomic gas. Proper relaxation of heat flux are achieved by selecting of the quantities ω_0 and ω_1,

$$\frac{\partial q_{tran}}{\partial t} = -\left(\frac{2}{3} + \frac{1-\omega_0}{3Zr}\right)\frac{P_{tran}}{\mu_{tran}} q_{tran},$$
$$\frac{\partial q_{rot}}{\partial t} = -\left[\sigma + \frac{(1-\sigma)(1-\omega_1)}{Zr}\right]\frac{P_{tran}}{\mu_{tran}} q_{tran}. \tag{5}$$

2.2. Reduced gas-kinetic models

The UGKS is a scheme for the capturing of time evolution of a gas distribution function $f(t, \mathbf{x}, \mathbf{u}, \epsilon)$, where the particle velocity space $\mathbf{u}$ is discretized and a continuous space is used for ϵ. In order to reduce the computational cost, reduced gas distribution functions can be defined,

$$G(t, \mathbf{x}, \mathbf{u}) = \int f(t, x, u, \epsilon)\, d\epsilon,$$
$$R(t, \mathbf{x}, \mathbf{u}) = \int \epsilon f(t, x, u, \epsilon)\, d\epsilon. \tag{6}$$

As a result, the relations between macroscopic flow variables and distribution functions can be written in terms of the moments of G and R,

$$W = \begin{pmatrix} \rho \\ \rho U \\ \rho V \\ \rho W \\ \rho E \\ \rho E_{rot} \end{pmatrix} = \int \begin{pmatrix} mG \\ muG \\ mvG \\ mwG \\ \frac{m(u^2+v^2+w^2)}{2} G + R \\ R \end{pmatrix} du\, dv\, dw. \tag{7}$$

Multiplying the Rykov equation by vector $(1, \epsilon)^T$ and integrating the vector equation in terms of the rotational energy, the following system can be obtained,

$$\frac{\partial G}{\partial t} + u\frac{\partial G}{\partial x} + v\frac{\partial G}{\partial y} + w\frac{\partial G}{\partial z} = \frac{G_{tran} - G}{\tau} + \frac{G_{rot} - G_{tran}}{Zr\tau},$$
$$\frac{\partial R}{\partial t} + u\frac{\partial R}{\partial x} + v\frac{\partial R}{\partial y} + w\frac{\partial R}{\partial z} = \frac{R_{tran} - R}{\tau} + \frac{R_{rot} - R_{tran}}{Zr\tau}, \tag{8}$$

where the evolution of the distribution function $f(t, \mathbf{x}, \mathbf{u}, \epsilon)$ is replaced by the time evolution of two new distribution functions G and R, which depend on $(t, \mathbf{x}, \mathbf{u})$ only. The above system (8) couples the time evolution of G and R through the collision terms. The equilibrium states in Eq. (8) depend on the macroscopic flow variables W in Eq. (7), which depend on G and R as well. These elastic and inelastic equilibrium states are denoted by G_{tran}, G_{rot}, R_{tran} and R_{rot}, which are given by

$$G_{tran} = \left[1 - \frac{2m\mathbf{q}_{tran}\cdot\mathbf{c}}{15kT_{tran}p_{tran}}\left(\frac{5}{2} - \frac{mc^2}{2kT_{tran}}\right)\right] G_{tran\_Guassian},$$
$$G_{rot} = \left[1 - \omega_0\frac{2m\mathbf{q}_{tran}\cdot\mathbf{c}}{15kTp}\left(\frac{5}{2} - \frac{mc^2}{2kT}\right)\right] G_{rot\_Gaussian},$$
$$R_{tran} = \left[1 - \frac{2m\mathbf{q}_{tran}\cdot\mathbf{c}}{15kT_{tran}p_{tran}}\left(\frac{5}{2} - \frac{mc^2}{2kT_{tran}}\right) + (1-\sigma)\frac{m\mathbf{q}_{rot}\cdot\mathbf{c}}{kT_{tran}p_{tran}}\right] R_{tran\_Guassian},$$
$$R_{rot} = \left[1 - \omega_0\frac{2m\mathbf{q}_{tran}\cdot\mathbf{c}}{15kTp}\left(\frac{5}{2} - \frac{mc^2}{2kT}\right) + \omega_1(1-\sigma)\frac{m\mathbf{q}_{rot}\cdot\mathbf{c}}{kTp}\right] R_{rot\_Gaussian}, \tag{9}$$

where $G_{tran\_Guassian}$, $G_{rot\_Gaussian}$, $R_{tran\_Guassian}$ and $R_{rot\_Gaussian}$ are Maxwellians defined by

$$G_{tran\_Guassian} = n\left(\frac{m}{2\pi kT_{tran}}\right)^{\frac{3}{2}} e^{-\frac{mc^2}{2kT_{tran}}},$$
$$G_{rot\_Guassian} = n\left(\frac{m}{2\pi kT}\right)^{\frac{3}{2}} e^{-\frac{mc^2}{2kT}},$$
$$R_{tran\_Guassian} = kT_{tran}G_{tran\_Guassian},$$
$$R_{rot\_Guassian} = kT_{rot}G_{rot\_Guassian}. \tag{10}$$

In Eq. (10), the distributions $G_{tran\_Guassian}$, $G_{rot\_Gaussian}$, $R_{tran\_Guassian}$, and $R_{rot\_Guassian}$ are fully determined by the macroscopic variables W in Eq. (7).

Defining

$$G_{eq} = \left(\frac{Zr-1}{Zr} G_{tran} + \frac{1}{Zr} G_{rot} \right),$$

and

$$R_{eq} = \left(\frac{Zr-1}{Zr} R_{tran} + \frac{1}{Zr} R_{rot} \right),$$

the system of model equations can be simplified as

$$\begin{aligned} &\frac{\partial G}{\partial t} + u\frac{\partial G}{\partial x} + v\frac{\partial G}{\partial y} + w\frac{\partial G}{\partial z} = \frac{(\frac{Zr-1}{Zr} G_{tran} + \frac{1}{Zr} G_{rot}) - G}{\tau} = \frac{G_{eq} - G}{\tau}, \\ &\frac{\partial R}{\partial t} + u\frac{\partial R}{\partial x} + v\frac{\partial R}{\partial y} + w\frac{\partial R}{\partial z} = \frac{(\frac{Zr-1}{Zr} R_{tran} + \frac{1}{Zr} R_{rot}) - R}{\tau} = \frac{R_{eq} - R}{\tau}. \end{aligned} \tag{11}$$

The construction of UGKS for diatomic gases will be based on the above equations.

2.3. Unified gas-kinetic scheme

Unified gas-kinetic scheme is a finite volume method. The physical space in 3D is divided into control volumes $\Omega_{i,j,k}$. The temporal discretization is denoted by t_n for the n-th time step. The particle velocity space is discretized in order to capture the non-equilibrium distribution. The discrete distribution functions in physical and velocity spaces are denoted by

$$\begin{aligned} G^n_{i,j,k} &= G^n_{i,j,k,\alpha,\beta,\gamma} = G(t_n, x_i, y_j, z_k, u_\alpha, v_\beta, w_\gamma), \\ R^n_{i,j,k} &= R^n_{i,j,k,\alpha,\beta,\gamma} = R(t_n, x_i, y_j, z_k, u_\alpha, v_\beta, w_\gamma). \end{aligned} \tag{12}$$

In order to simplify the notation, the index α, β, γ for the discrete particle velocity will be omitted for convenience. With the discrete particle velocity points, the moments of gas distribution functions have to be done by numerical quadrature over velocity space,

$$W^n_{i,j,k} = \sum \begin{pmatrix} mG^n_{i,j,k}\kappa_1(u,v,w) \\ muG^n_{i,j,k}\kappa_u(u,v,w) \\ mvG^n_{i,j,k}\kappa_v(u,v,w) \\ mwG^n_{i,j,k}\kappa_w(u,v,w) \\ (\frac{m(u^2+v^2+w^2)}{2} G^n_{i,j,k} + R^n_{i,j,k})\kappa_e(u,v,w) \\ R^n_{i,j,k}\kappa_r(u,v,w) \end{pmatrix}, \tag{13}$$

where κ_1, κ_u, κ_v, κ_w, κ_e and κ_r are the weights for numerical quadratures. The UGKS method is constructed in the following.

(i) Integrating the model Eq. (8) over the control volume $\Omega_{i,j,k}$ in a physical space and in a time interval (t_n, t_{n+1}).
(ii) Discretizing the time integration of collision terms using a trapezoid rule.
(iii) Using the following two equations for updating the gas distribution functions ($G_{i,j,k}$ and $R_{i,j,k}$) and macroscopic flow variables (W) in the control volume $\Omega_{i,j,k}$,

$$G^{n+1}_{i,j,k} = G^n_{i,j,k} + \frac{1}{\Omega_{i,j,k}} \int_{t_n}^{t_{n+1}} \oint_{\partial\Omega_{i,j,k}} G_{cf}(u,t)\mathbf{u}\cdot d\mathbf{S}\,dt + \frac{\Delta t}{\Omega_{i,j,k}} \left(\frac{G^n_{eq,i,j,k} - G^n_{i,j,k}}{2\tau^n} + \frac{G^{n+1}_{eq,i,j,k} - G^{n+1}_{i,j,k}}{2\tau^{n+1}} \right), \tag{14}$$

$$R^{n+1}_{i,j,k} = R^n_{i,j,k} + \frac{1}{\Omega_{i,j,k}} \int_{t_n}^{t_{n+1}} \oint_{\partial\Omega_{i,j,k}} R_{cf}(u,t)\mathbf{u}\cdot d\mathbf{S}\,dt + \frac{\Delta t}{\Omega_{i,j,k}} \left(\frac{R^n_{eq,i,j,k} - R^n_{i,j,k}}{2\tau^n} + \frac{R^{n+1}_{eq,i,j,k} - R^{n+1}_{i,j,k}}{2\tau^{n+1}} \right), \tag{15}$$

$$W^{n+1}=\begin{pmatrix}\rho\\ \rho U\\ \rho V\\ \rho W\\ \rho E\\ \rho E_{rot}\end{pmatrix}_{i,j,k}^{n+1}=\begin{pmatrix}\rho\\ \rho U\\ \rho V\\ \rho W\\ \rho E\\ \rho E_{rot}\end{pmatrix}_{i,j,k}^{n}+\frac{1}{\Omega_{i,j,k}}\sum\int_{t_n}^{t_{n+1}}\oint_{\partial\Omega_{i,j,k}}\left[\begin{pmatrix}m\\ mu\\ mv\\ mw\\ m(\frac{u^2+v^2+w^2}{2})\\ 0\end{pmatrix}G_{cf}(u,t)+\begin{pmatrix}0\\0\\0\\0\\1\\1\end{pmatrix}R_{cf}(u,t)\right]\mathbf{u}\cdot d\mathbf{S}\,dt\,d\Xi+\begin{pmatrix}0\\0\\0\\0\\0\\ \Delta t(\frac{(\rho E_{rot})^n-(\rho E_{rot,eq})^n}{2\tau^n}+\frac{(\rho E_{rot})^{n+1}-(\rho E_{rot,eq})^{n+1}}{2\tau^{n+1}})\end{pmatrix}. \tag{16}$$

In the above system, in order to update the gas distribution functions in Eqs. (14) and (15), the equilibrium states ($G_{eq,i,j,k}^{n+1}$ and $R_{eq,i,j,k}^{n+1}$) at $(n+1)$-th time step depend on the macroscopic flow variables at $(n+1)$-th step, which can be provided through the solution of Eq. (16). Therefore, the solutions in Eqs. (14), (15), and (16) can be uniquely determined once the time dependent gas distribution functions $G_{cf}(\mathbf{u},t)$ and $R_{cf}(\mathbf{u},t)$ at a cell interface (cf refers to cell interface) can be obtained. The construction of the cell interface gas distribution function is the central point in the development of UGKS.

In UGKS method, the cell interface (cf) time evolution distribution functions $G_{cf}(\mathbf{u},t)$ and $R_{cf}(\mathbf{u},t)$ are modeled by the local analytical solution of kinetic equations (11). The time evolution solutions are

$$\begin{aligned}G_{cf}(t,\mathbf{u})&=G(t,\mathbf{u},\mathbf{x}_{cf})=\frac{1}{\tau}\int_{t_n}^{t}G_{eq}\big(t',\mathbf{u},\mathbf{x}_{cf}-\mathbf{u}t+\mathbf{u}t'\big)e^{\frac{t'-t}{\tau}}\,dt'+e^{\frac{t_n-t}{\tau}}G\big(t_n,\mathbf{u},\mathbf{x}_{cf}-\mathbf{u}(t-t_n)\big),\\ R_{cf}(t,\mathbf{u})&=R(t,\mathbf{u},\mathbf{x}_{cf})=\frac{1}{\tau}\int_{t_n}^{t}R_{eq}\big(t',\mathbf{u},\mathbf{x}_{cf}-\mathbf{u}t+\mathbf{u}t'\big)e^{\frac{t'-t}{\tau}}\,dt'+e^{\frac{t_n-t}{\tau}}R\big(t_n,\mathbf{u},\mathbf{x}_{cf}-\mathbf{u}(t-t_n)\big),\end{aligned} \tag{17}$$

where $G(t_n,\mathbf{u},\mathbf{x}_{cf}-\mathbf{u}(t-t_n))$ and $R(t_n,\mathbf{u},\mathbf{x}_{cf}-\mathbf{u}(t-t_n))$ are the initial condition of the distribution functions. The solutions are actually a weighted averaging of initial free transport and the equilibrium state evolution. In other words, it is a crossing scale solution from the kinetic to the hydrodynamic ones.

The initial gas distribution functions can be obtained through the Taylor expansion around the point $(t_n,\mathbf{u},\mathbf{x}_{cf})$, the superscript l and r denote the left-hand side and right-hand side of a cell interface,

$$\begin{aligned}G(t_n,\mathbf{u},\mathbf{x}_{cf}-\mathbf{u}t)&=\big(1-H[-\mathbf{u}\cdot\mathbf{S}]\big)G^l(t_n,\mathbf{u},\mathbf{x}_{cf})+H[-\mathbf{u}\cdot\mathbf{S}]G^r(t_n,\mathbf{u},\mathbf{x}_{cf})\\ &\quad+\big(1-H[-\mathbf{u}\cdot\mathbf{S}]\big)\frac{\partial G}{\partial\mathbf{x}}\Big|^{l}_{(t_n,\mathbf{u},\mathbf{x}_{cf})}\cdot\big(-\mathbf{u}(t-t_n)\big)+H[-\mathbf{u}\cdot\mathbf{S}]\frac{\partial G}{\partial\mathbf{x}}\Big|^{r}_{(t_n,\mathbf{u},\mathbf{x}_{cf})}\cdot\big(-\mathbf{u}(t-t_n)\big),\\ R(t_n,\mathbf{u},\mathbf{x}_{cf}-\mathbf{u}t)&=\big(1-H[-\mathbf{u}\cdot\mathbf{S}]\big)R^l(t_n,\mathbf{u},\mathbf{x}_{cf})+H[-\mathbf{u}\cdot\mathbf{S}]R^r(t_n,\mathbf{u},\mathbf{x}_{cf})\\ &\quad+\big(1-H[-\mathbf{u}\cdot\mathbf{S}]\big)\frac{\partial R}{\partial\mathbf{x}}\Big|^{l}_{(t_n,\mathbf{u},\mathbf{x}_{cf})}\cdot\big(-\mathbf{u}(t-t_n)\big)+H[-\mathbf{u}\cdot\mathbf{S}]\frac{\partial R}{\partial\mathbf{x}}\Big|^{r}_{(t_n,\mathbf{u},\mathbf{x}_{cf})}\cdot\big(-\mathbf{u}(t-t_n)\big),\end{aligned} \tag{18}$$

where $\mathbf{S}$ is the unit normal direction of a cell interface, $G^{l,r}(t_n,\mathbf{u},\mathbf{x}_{cf})$, $R^{l,r}(t_n,\mathbf{u},\mathbf{x}_{cf})$ are the distributions at the cell interface at time t_n. With the definition of $\mathbf{x}_{cc}^l$ as the location of cell center (cc) on the left-hand side of a cell interface, and $\mathbf{x}_{cc}^r$ on the right-hand side, the reconstructed values at the cell interface (cf) can be expressed as

$$\begin{aligned}G^l(t_n,\mathbf{u},\mathbf{x}_{cf})&=G^n\big(t_n,\mathbf{u},\mathbf{x}_{cc}^l\big)+\frac{\partial G}{\partial\mathbf{x}}\Big|^{l}_{(t_n,\mathbf{u},\mathbf{x}_{cc}^l)}\cdot\big(\mathbf{x}_{cf}-\mathbf{x}_{cc}^l\big),\\ G^r(t_n,\mathbf{u},\mathbf{x}_{cf})&=G^n\big(t_n,\mathbf{u},\mathbf{x}_{cc}^r\big)+\frac{\partial G}{\partial\mathbf{x}}\Big|^{r}_{(t_n,\mathbf{u},\mathbf{x}_{cc}^r)}\cdot\big(\mathbf{x}_{cf}-\mathbf{x}_{cc}^r\big),\end{aligned}$$

$$R^l(t_n,\mathbf{u},\mathbf{x}_{cf}) = R^n\big(t_n,\mathbf{u},\mathbf{x}^l_{cc}\big) + \left.\frac{\partial R}{\partial \mathbf{x}}\right|^l_{(t_n,\mathbf{u},\mathbf{x}^l_{cc})} \cdot \big(\mathbf{x}_{cf}-\mathbf{x}^l_{cc}\big),$$
$$R^r(t_n,\mathbf{u},\mathbf{x}_{cf}) = R^n\big(t_n,\mathbf{u},\mathbf{x}^r_{cc}\big) + \left.\frac{\partial R}{\partial \mathbf{x}}\right|^r_{(t_n,\mathbf{u},\mathbf{x}^r_{cc})} \cdot \big(\mathbf{x}_{cf}-\mathbf{x}^r_{cc}\big). \tag{19}$$

The distributions at cell center, such as $G^n(t_n,\mathbf{u},\mathbf{x}^l_{cc})$, $G^n(t_n,\mathbf{u},\mathbf{x}^r_{cc})$, $R^n(t_n,\mathbf{u},\mathbf{x}^l_{cc})$ and $R^n(t_n,\mathbf{u},\mathbf{x}^r_{cc})$ are the cell averaged values. In this paper, a second order reconstruction scheme is used to get slopes inside each control volume,

$$\left.\frac{\partial G}{\partial \mathbf{x}}\right|^l_{(t_n,\mathbf{u},\mathbf{x}_{cf})} = \left.\frac{\partial G}{\partial \mathbf{x}}\right|^l_{(t_n,\mathbf{u},\mathbf{x}^l_{cc})}, \qquad \left.\frac{\partial G}{\partial \mathbf{x}}\right|^r_{(t_n,\mathbf{u},\mathbf{x}_{cf})} = \left.\frac{\partial G}{\partial \mathbf{x}}\right|^r_{(t_n,\mathbf{u},\mathbf{x}^r_{cc})},$$
$$\left.\frac{\partial R}{\partial \mathbf{x}}\right|^l_{(t_n,\mathbf{u},\mathbf{x}_{cf})} = \left.\frac{\partial R}{\partial \mathbf{x}}\right|^l_{(t_n,\mathbf{u},\mathbf{x}^l_{cc})}, \qquad \left.\frac{\partial R}{\partial \mathbf{x}}\right|^r_{(t_n,\mathbf{u},\mathbf{x}_{cf})} = \left.\frac{\partial R}{\partial \mathbf{x}}\right|^r_{(t_n,\mathbf{u},\mathbf{x}^r_{cc})}. \tag{20}$$

The gradients of distribution functions in Eq. (20) are constructed by the differences of cell averaged values and with the application of nonlinear limiter [40].

The equilibrium states in the integral solution are expanded in the following,

$$\begin{aligned}
&G_{eq}\big(t',\mathbf{u},\mathbf{x}_{cf}-\mathbf{u}(t-t')\big)\\
&= \frac{Zr-1}{Zr}\big\{G_{tran}(t_n,\mathbf{u},\mathbf{x}_{cf}) + \big[\big(1-H\big[\mathbf{x}'\cdot\mathbf{S}\big]\big)\mathbf{a}^l_G\cdot\mathbf{x}' + \big(H\big[\mathbf{x}'\cdot\mathbf{S}\big]\big)\mathbf{a}^r_G\cdot\mathbf{x}' + A_G t'\big]G_{tran_Guassian}(t_n,\mathbf{u},\mathbf{x}_{cf})\big\}\\
&\quad + \frac{1}{Zr}\big\{G_{rot}(t_n,\mathbf{u},\mathbf{x}_{cf}) + \big[\big(1-H\big[\mathbf{x}'\cdot\mathbf{S}\big]\big)\mathbf{b}^l_G\cdot\mathbf{x}' + \big(H\big[\mathbf{x}'\cdot\mathbf{S}\big]\big)\mathbf{b}^r_G\cdot\mathbf{x}' + B_G t'\big]G_{rot_Guassian}(t_n,\mathbf{u},\mathbf{x}_{cf})\big\},\\
&R_{eq}\big(t',\mathbf{u},\mathbf{x}_{cf}-\mathbf{u}(t-t')\big)\\
&= \frac{Zr-1}{Zr}\big\{R_{tran}(t_n,\mathbf{u},\mathbf{x}_{cf}) + \big[\big(1-H\big[\mathbf{x}'\cdot\mathbf{S}\big]\big)\mathbf{a}^l_R\cdot\mathbf{x}' + \big(H\big[\mathbf{x}'\cdot\mathbf{S}\big]\big)\mathbf{a}^r_R\cdot\mathbf{x}' + A_R t'\big]R_{tran_Guassian}(t_n,\mathbf{u},\mathbf{x}_{cf})\big\}\\
&\quad + \frac{1}{Zr}\big\{R_{rot}(t_n,\mathbf{u},\mathbf{x}_{cf}) + \big[\big(1-H\big[\mathbf{x}'\cdot\mathbf{S}\big]\big)\mathbf{b}^l_R\cdot\mathbf{x}' + \big(H\big[\mathbf{x}'\cdot\mathbf{S}\big]\big)\mathbf{b}^r_R\cdot\mathbf{x}' + B_R t'\big]R_{rot_Guassian}(t_n,\mathbf{u},\mathbf{x}_{cf})\big\},
\end{aligned} \tag{21}$$

where $\mathbf{x}' = \mathbf{x}_{cf} - \mathbf{u}(t-t')$. Vectors $\mathbf{a}^l_G, \mathbf{a}^r_G, \mathbf{b}^l_G, \mathbf{b}^r_G, \mathbf{a}^l_R, \mathbf{a}^r_R, \mathbf{b}^l_R, \mathbf{b}^r_R$ are related to the spatial gradients of equilibrium states. As an example, $\mathbf{a}^l_G$ is related to the spatial gradient of the equilibrium state of elastic collisions on the left-hand side of a cell interface, and it is formulated as

$$\mathbf{a}^l_G G_{tran\_Guassian}(t_n,\mathbf{u},\mathbf{x}_{cf}) = \left.\frac{\partial G_{tran\_Guassian}}{\partial \mathbf{x}}\right|^l_{(t_n,\mathbf{u},\mathbf{x}_{cf})}, \tag{22}$$

with the components

$$\begin{aligned}
a^l_{G,x} &= a^l_{G,x,1} + a^l_{G,x,2}u + a^l_{G,x,3}v + a^l_{G,x,4}w + a^l_{G,x,5}\big(u^2+v^2+w^2\big),\\
a^l_{G,y} &= a^l_{G,y,1} + a^l_{G,y,2}u + a^l_{G,y,3}v + a^l_{G,y,4}w + a^l_{G,y,5}\big(u^2+v^2+w^2\big),\\
a^l_{G,z} &= a^l_{G,z,1} + a^l_{G,z,2}u + a^l_{G,z,3}v + a^l_{G,z,4}w + a^l_{G,z,5}\big(u^2+v^2+w^2\big).
\end{aligned}$$

Here A_G, B_G, A_R and B_R are defined as the time variations of the equilibrium states. For example, $\mathbf{A}_G$ is related to the time derivative of the equilibrium state of the elastic collisions,

$$A_G G_{tran\_Guassian}(t_n,\mathbf{u},\mathbf{x}_{cf}) = \left.\frac{\partial G_{tran\_Guassian}}{\partial t}\right|_{(t_n,\mathbf{u},\mathbf{x}_{cf})}, \tag{23}$$

where

$$A^l_G = A^l_{G,1} + A^l_{G,2}u + A^l_{G,3}v + A^l_{G,4}w + A^l_{G,5}\big(u^2+v^2+w^2\big).$$

The equilibrium states and their derivatives are fully determined by macroscopic variables and their gradients. Consequently, the slopes of $\mathbf{a}^l_G$, $\mathbf{a}^r_G$, $\mathbf{b}^l_G$, $\mathbf{b}^r_G$, A_G, and B_G can be fully calculated in the following way.

Suppose that αG represents the spatial or temporal derivative of an equilibrium state G, with the coefficients $\alpha = \alpha_1 + \alpha_2 u + \alpha_3 v + \alpha_4 w + \alpha_5(u^2+v^2+w^2)$, and the corresponding macroscopic variables and their derivatives in the equilibrium state G are given, such as ρ', U', V', W', λ' for the spatial or temporal derivatives of the corresponding macroscopic

variables ρ, U, V, W, λ, then the coefficients in α are given by

$$\begin{aligned}
\alpha_1 &= \frac{2\lambda\rho' + \rho(-4\lambda^2(UU' + VV' + WW') + (3 - 2(U^2 + V^2 + W^2)\lambda)\lambda')}{2\rho\lambda}, \\
\alpha_2 &= 2\left(\lambda U' + U\lambda'\right), \\
\alpha_3 &= 2\left(\lambda V' + V\lambda'\right), \\
\alpha_4 &= 2\left(\lambda W' + W\lambda'\right), \\
\alpha_5 &= -\lambda',
\end{aligned} \tag{24}$$

where $\lambda = m/2kT_{tran}$ for $\mathbf{a}_G^l, \mathbf{a}_G^r$ and A_G; and $\lambda = m/2kT$ for $\mathbf{b}_G^l, \mathbf{b}_G^r$ and B_G. Similarly, with βR for the spatial or temporal derivative of an equilibrium state R, and the coefficients $\beta = \beta_1 + \beta_2 u + \beta_3 v + \beta_4 w + \beta_5(u^2 + v^2 + w^2)$, these coefficients are determined by

$$\begin{aligned}
\beta_1 &= \alpha_1 - \frac{\lambda'}{\lambda}, \\
\beta_2 &= \alpha_2, \\
\beta_3 &= \alpha_3, \\
\beta_4 &= \alpha_4, \\
\beta_5 &= \alpha_5,
\end{aligned} \tag{25}$$

where $\lambda = m/2kT_{tran}$ for $\mathbf{a}_R^l, \mathbf{a}_R^r$ and A_R; and $\lambda = m/2kT$ for $\mathbf{b}_R^l, \mathbf{b}_R^r$, and B_R. The spatial derivatives of macroscopic variables inside each cell can be obtained through the reconstruction of macroscopic flow variables with the application of nonlinear limiter. Therefore, all above spatial derivatives for ρ, U, V, W, λ are known. In order to get the time derivatives for ρ, U, V, W, λ, we need to do the following. Taking conservative moments on the kinetic equation, due to the vanishing of collision term to the conservative moments, the moments of the temporal and spatial derivatives of a distribution function are connected. This is also applicable to the equilibrium states. With the definitions $\psi_1 = (m, mu, mv, mw, \frac{m(u^2+v^2+w^2)}{2}, 0)^T$ and $\psi_2 = (0, 0, 0, 0, 1, 1)^T$, we have

$$\int \left[\psi_1 \left(\frac{\partial G_{tran}}{\partial t} + \mathbf{u} \cdot \frac{\partial G_{tran}}{\partial \mathbf{x}} \right) + \psi_2 \left(\frac{\partial R_{tran}}{\partial t} + \mathbf{u} \cdot \frac{\partial R_{tran}}{\partial \mathbf{x}} \right) \right] d\Xi = 0. \tag{26}$$

Consequently, the temporal derivatives of macroscopic variables can be obtained as

$$\frac{\partial W}{\partial t} = -\int \left[\begin{pmatrix} m \\ mu \\ mv \\ mw \\ m(\frac{u^2+v^2+w^2}{2}) \\ 0 \end{pmatrix} \left(\mathbf{u} \cdot \frac{\partial G_{tran}}{\partial \mathbf{x}} \right) + \begin{pmatrix} 0 \\ 0 \\ 0 \\ 0 \\ 1 \\ 1 \end{pmatrix} \left(\mathbf{u} \cdot \frac{\partial R_{tran}}{\partial \mathbf{x}} \right) \right] d\Xi. \tag{27}$$

Then, based on the above time derivative of macroscopic flow variables, the temporal derivatives of distribution functions are fully determined using Eq. (23).

The numerical procedures of UGKS for diatomic gas are identical to the UGKS for monatomic gas, except the inclusion of additional rotational degree of freedom. The corresponding numerical procedures for monatomic gas are given in [20]. At end, we present a summary of the unified gas-kinetic scheme for diatomic gases:

1. The Rykov model equation is split into two equations for reduced distribution functions.
2. The time evolution of distribution functions at a cell interface are modeled by the integral solutions of the Rykov equations.
3. The initial condition and the integration of equilibrium states are determined explicitly in the above integral solutions for the flux evaluation. The macroscopic conservative flow variables inside each cell are updated first using the above integral solutions for the flux evaluation.
4. A finite volume scheme is developed for the update of gas distribution functions with fluxes from the above integral solutions, and with the source terms treatment inside each cell, where the updated macroscopic variables are used for the determination of the equilibrium states of the source terms.

At end, we discuss the rotational collision number for the diatomic gas. The energy relaxation term of Rykov equation is modeled using a Landau–Teller–Jeans relaxation. The particle collision time multiplied by rotational collision number Z_r

defines the relaxation rate for the rotational energy equilibrating with the translational energy. In the current paper, the value Z_r used is,

$$Z_r = \frac{Z_r^*}{1 + (\pi^{3/2}/2)\sqrt{\tilde{T}/T_{tran}} + (\pi + \pi^2/4)(\tilde{T}/T_{tran})}, \tag{28}$$

where the quantity $\tilde{T}$ is the characteristic temperature of intermolecular potential, and Z_r^* has a fixed value. Over a temperature range from 30 K to 3000 K for N_2, a value $Z_r^* = 23.0$ and $\tilde{T} = 91.5$ K are used. More complicated models for the energy relaxation can be found in [41–44].

3. Analysis of UGKS

The initial conditions in Eq. (11) are $G(t_n, \mathbf{u}, \mathbf{x})$ and $R(t_n, \mathbf{u}, \mathbf{x})$. In the collisionless limit, i.e., $\tau \to \infty$, the analytical solutions at a cell interface become

$$\begin{aligned} G_{cf}(t, \mathbf{u}) &= G\big(t_n, \mathbf{u}, \mathbf{x}_{cf} - \mathbf{u}(t - t_n)\big), \\ R_{cf}(t, \mathbf{u}) &= R\big(t_n, \mathbf{u}, \mathbf{x}_{cf} - \mathbf{u}(t - t_n)\big). \end{aligned} \tag{29}$$

As a free molecular flow, the above solution is exact.

For the equilibrium flow, there are intensive particle collisions. As a result of $\Delta t \gg \tau$, the gas distribution functions at a cell interface become

$$\frac{1}{\tau}\int_{t_n}^{t_n+\Delta t} G_{eq}\big(t', \mathbf{u}, \mathbf{x}_{cf} - \mathbf{u}\big(t - t'\big)\big) e^{\frac{t'-t}{\tau}}\, dt'$$

and

$$\frac{1}{\tau}\int_{t_n}^{t_n+\Delta t} R_{eq}\big(t', \mathbf{u}, \mathbf{x}_{cf} - \mathbf{u}\big(t - t'\big)\big) e^{\frac{t'-t}{\tau}}\, dt',$$

which precisely present the NS solutions of the Chapman–Enskog expansion. This is the hydrodynamic limits of the UGKS. Therefore, the integral solution in UGKS makes an automatic adaptation between the kinetic and hydrodynamic scales flow evolution. For the DVM, only the solution in Eq. (29) is used as the cell interface gas distribution function, which has no particle collisions involved. Therefore, it is basically valid in the kinetic scale. DSMC has the same property. However, the integral solution used in UGKS pushes its applicable regime beyond the kinetic scale modeling. With this property, the UGKS has the advantage of using a much larger time step. A large time step is of great importance for simulating flow in transition and continuum flow regimes, especially the cases with high Reynolds numbers.

For diatomic gases, in the continuum limit the Navier–Stokes equations with bulk viscosity will be recovered from the kinetic model equations. The bulk viscosity formulation is the limiting case when the translational and rotational temperature are close to each other. In the cases with limited amount difference between translational and rotational temperature, instead of the bulk viscosity expression for the stress the general constitutive relationship in the near continuum limit will be associated with the temperature differences [36,37,39].

4. Numerical examples

4.1. Rotational relaxation in a homogeneous gas

For a diatomic homogeneous gas with different initial rotational T_{rot} and translational temperature T_{tran}, the system will evolve into an equilibrium one with average temperature T, which is a constant. Intermolecular collision will relax T_{rot} to an averaged temperature T with a rate related to the collision frequency. Due to the homogeneous space distribution, the governing equations can be simplified as

$$\frac{\partial f}{\partial t} = \frac{g_{tran} - f}{\tau} + \frac{g_{rot} - g_{tran}}{Zr\tau}. \tag{30}$$

Multiplying the above equation with ϵ and integrating over the whole velocity and rotational energy space, the time evolution of rotational energy can be obtained,

$$\frac{\partial T_{rot}}{\partial t} = \frac{T - T_{rot}}{Zr\tau}. \tag{31}$$

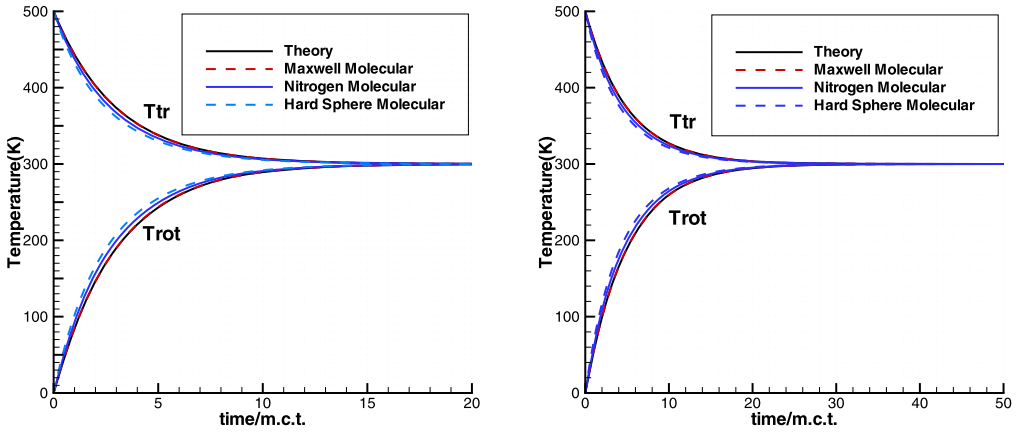

(a) *case with* $Z_r = 3$ (b) *case with* $Z_r = 5$

Fig. 1. Rotational relaxation in a homogeneous gas.

In the case with constant rotational collision number Z_r and mean collision time τ, an analytical solution of Eq. (31) can be obtained,

$$T_{rot}(t) = T - \big(T - T_{rot}(0)\big)e^{-\frac{t}{Zr\tau}}. \tag{32}$$

For real diatomic gas, the mean collision time depends on the transitional temperature even in the homogeneous case. For the VHS model, the collision time can be approximated as $\tau = \mu/p \sim T^{\omega}_{tran}/(\rho R T_{tran})$, which is a constant only for the Maxwell molecule with $\omega = 1$. For hard sphere ($\omega = 1/2$) and nitrogen ($\omega = 0.72$), τ depends on the temperature and there is no exact analytical solution. In this test, only one cell in physical space is used with periodic boundary condition. The domain in velocity space $(u, v) \in [(-5, 5) \times (-5, 5)]$ is discretized with 50×50 mesh points. Figs. 1(a) and 1(b) present the UGKS solutions at $Zr = 3$ and 5 for Maxwell, hard sphere, and nitrogen molecules along with the analytic solution (Maxwell gas only), where the mean collision time (m.c.t.) is calculated using the averaging temperature T in all three cases to normalize the time. The UGKS solution for the Maxwell molecule matches completely with the theoretical prediction. The collision frequencies for the HS and VHS models are higher than the Maxwell one, and they present faster relaxation to the equilibrium state.

4.2. Shock structure

For the nitrogen gas, the viscosity in DSMC simulations is calculated with VHS model ($\omega = 0.72$), and the collision rotation number Z_r is set as a constant. The collision time τ depends on the translational temperature only, it is determined with the same formula as the argon gas [20]. The collision rotation number Zr used in the UGKS has a value $Z_r = 2.4$. The temperature and density comparisons between UGKS and DSMC at $Ma = 1.53$, 4.0, 5.0 and 7.0 are plotted in Fig. 2. As $Z_r \to \infty$, the Rykov model reduces to the Shakhov model. For all relaxation type kinetic models, at high Mach number the translational temperature in the shock structure always goes up earlier in comparison with the DSMC results [21]. The main reason is that the relaxation model equally re-distributes the energy of high speed particles close to the upstream to all molecules there through a single relaxation time. In reality, the high speed particles at the upstream can transport a longer distance than low speed particles before encountering particle collisions. Therefore, it seems that the relaxation models can thermalize more efficiently the energy among all particles and raise the temperature earlier. But, based on all previous tests, the density distributions in the shock structures from the kinetic relaxation models can match with the DSMC solutions very well. Based on the same coefficients, the comparison of density profiles at different Mach numbers between UGKS and experimental data [45] are illustrated in Fig. 3.

4.3. Flow passing a flat plate

Space vehicles, space stations, and planetary exploration systems fly in a rarefied gas environment. Due to the hypersonic velocity, their flight environment includes shock-shock interactions and shock-boundary interactions that cause high heat transfer and pressure on the body of the spacecraft. Strong thermal non-equilibrium is associated with these flows. It is important to study the physical flow around spacecraft in a hypersonic rarefied environment in order to understand flow phenomenon and to design a real size vehicle. Here following the experiment [46], we are going to simulate the hypersonic rarefied gas flow over a flat plate, and compare our simulation results with the experimental measurements. The early study of this case has been done using the gas-kinetic scheme with multiple temperature model [39].

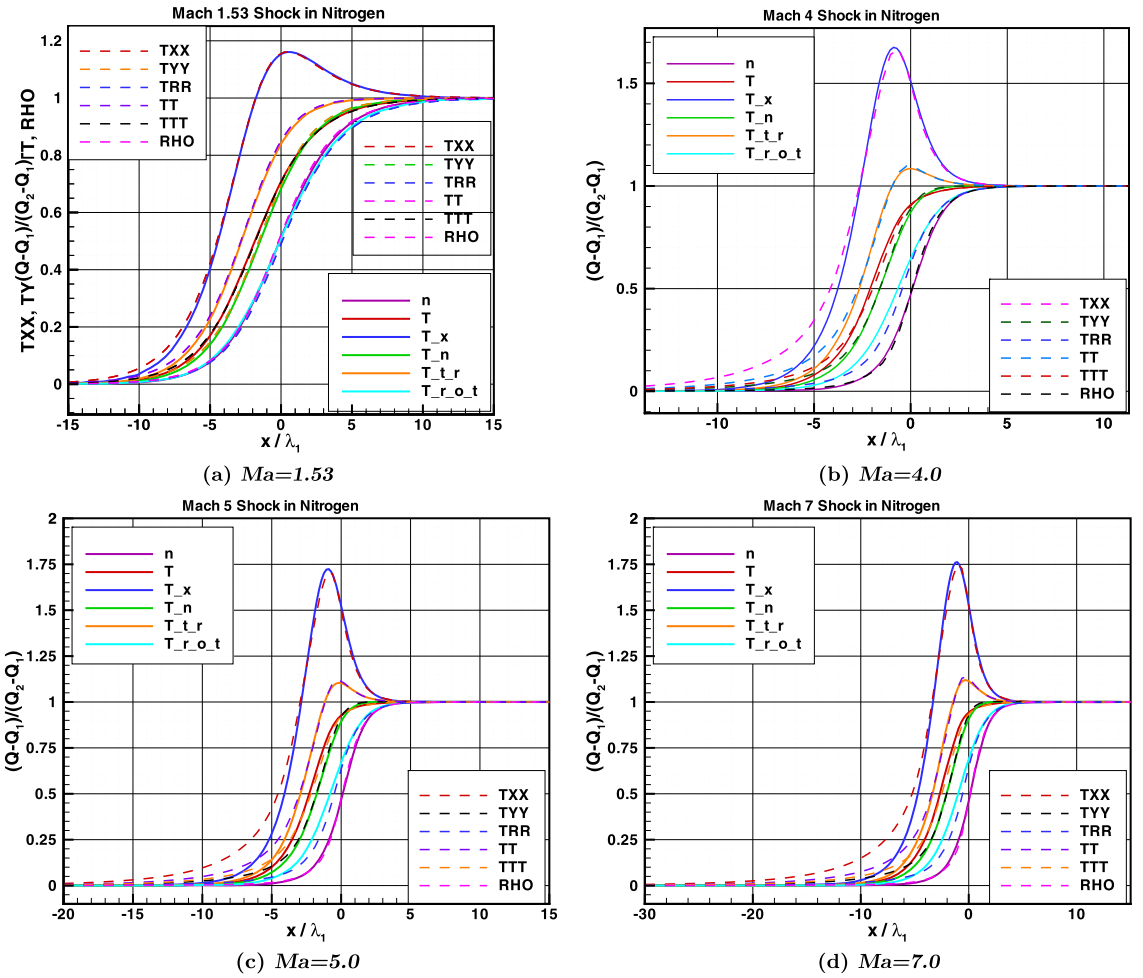

Fig. 2. Comparison of UGKS and DSMC solutions at different Mach numbers.

Table 1
The condition in run34 case in Ref. [46] and non-dimensional system.

Condition in run34 case		Non-dimensional coefficients	
Nozzle exit Mach number	4.89	length L_{ref}	1 mm
Nozzle exit temperature T_e	116 K	density ρ_{ref}	ρ_e
Nozzle exit static pressure P_e	2.12 Pa	velocity V_{ref}	$\sqrt{2R_{specical}T_e}$
Stagnation temperature T_0	670 K	temperature T_{ref}	T_e
Stagnation pressure P_0	983 Pa	energy e_{ref}	$\rho_e T_e$
Surface temperature T_w	290 K		

The run34 case in [46] will be studied, where the condition is shown in Table 1. The flat plate is made of copper and is cooled by water to preserve a constant wall temperature 290 K. The mean free path λ_{mfp} and viscosity coefficient μ are defined as

$$\lambda_{mfp} = \frac{16}{5}\left(\frac{1}{2\pi RT}\right)^{1/2}\frac{\mu}{\rho}, \tag{33}$$

and

$$\mu = \mu_0\left(\frac{T}{T_0}\right)^{\omega}. \tag{34}$$

The gas constant R and viscosity index ω of nitrogen gas are given by 297 $\mathrm{J\,kg^{-1}\,K^{-1}}$ and 0.75. Therefore, the density at nozzle exit can be determined, i.e., ρ_{ref} is 6.15×10^{-5} $\mathrm{kg\,m^{-3}}$.

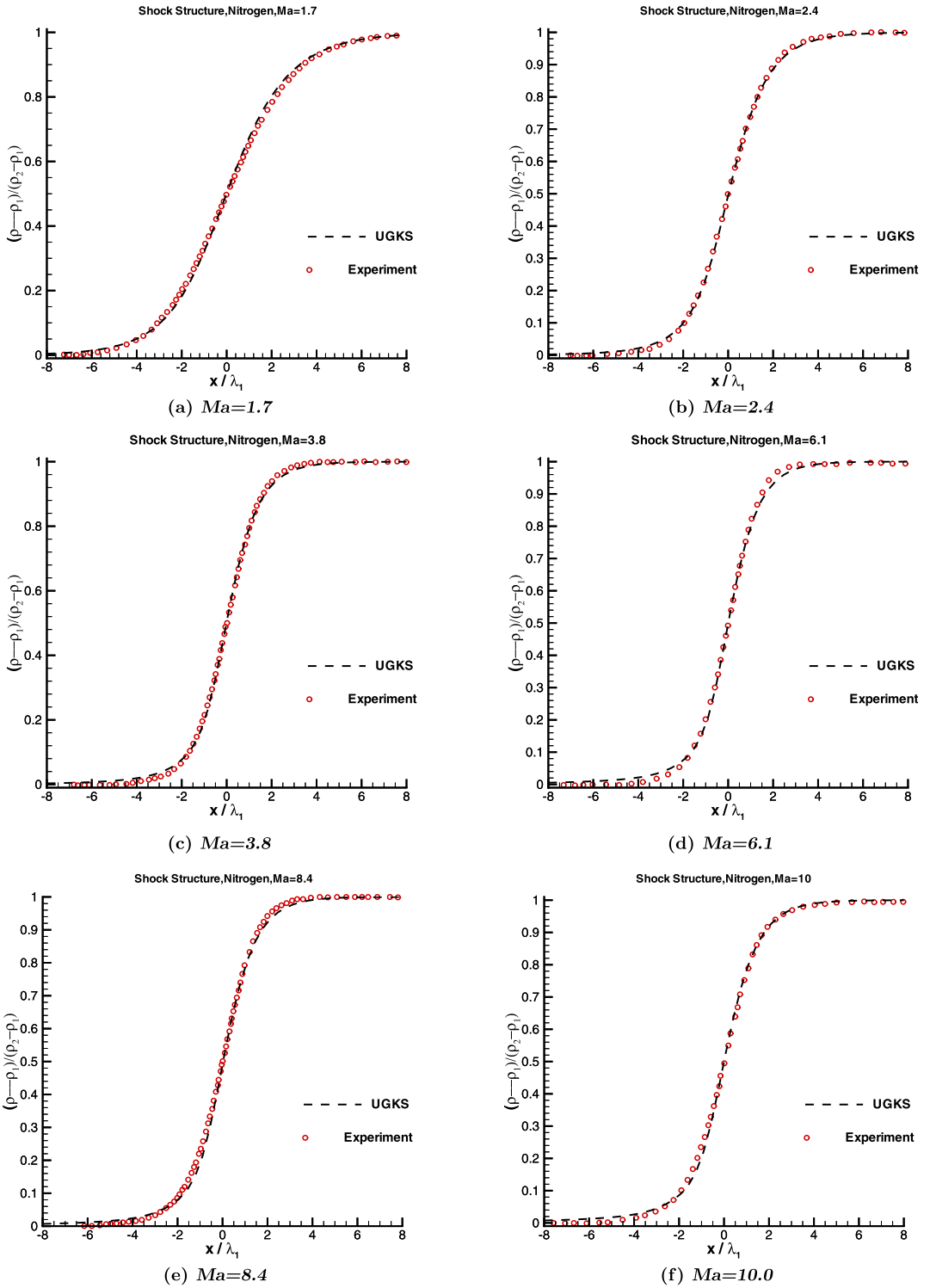

(a) $Ma=1.7$ (b) $Ma=2.4$

(c) $Ma=3.8$ (d) $Ma=6.1$

(e) $Ma=8.4$ (f) $Ma=10.0$

Fig. 3. Density profiles of experiment measurements and UGKS solutions at different Mach numbers.

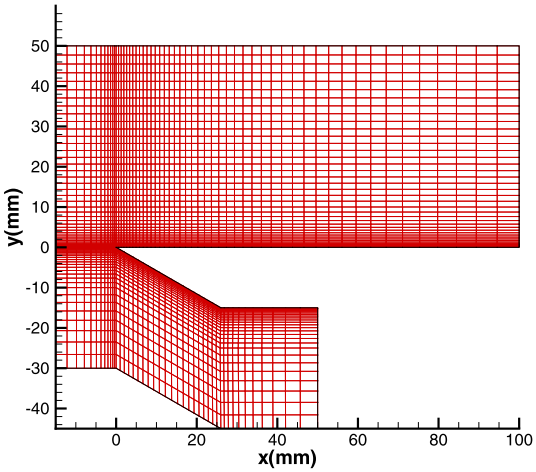

Fig. 4. Computational Mesh for the flat plate simulation.

At inlet boundary, the inflow gas has a Maxwellian distribution. The outlet boundary uses a non-reflection boundary condition, where the flow distribution outside domain is extrapolated from the interior region. The interaction between the gas flow and the solid boundary is the Maxwell boundary condition with full accommodation, which has been widely used [47–49].

In this study, the shock wave and boundary layer at the sharp leading edge are merged. Highly non-equilibrium between translational and rotational temperatures appears above the flat plate. In the experiment, the non-equilibrium rotational temperatures were measured by an electron beam fluorescence technique [46]. The UGKS used in this case is the second order scheme and the cell size of the UGKS is not limited by the mean free path, thus a relatively coarse mesh is used to obtain the result. Here 3323 elements are used in physical space with 59×39 mesh points above the plate and 44×25 below the plate, which is shown in Fig. 4. The CFL number is set to be 0.5. The domain in velocity space $(u, v) \in [(-10, 10) \times (-8, 8)]$ is discretized with 80×60 mesh points. Fig. 5 presents the density, translational, rotational, and total temperature contours around the sharp edged flat plate. The temperature distributions along the vertical line above the flat plate at the locations of $x = 5$ mm and $x = 20$ mm from the leading edge are presented in Fig. 6. The numerical results match well with the experimental data. The distribution function contours in the vertical direction at $x = 5$ mm and $x = 20$ mm are shown in Figs. 7 and 8 respectively.

4.4. Flow around a blunt circular cylinder

In this case, we consider the hypersonic flow passes through a blunt cylinder at $Ma = 5.0$ and $Kn = 0.1$. Just as shown in Fig. 9, the cylinder radius has a value 0.01 m, and the computational domain is divided with 10,000 and 4900×2 quadrilateral cells for DSMC (half domain) and UGKS (whole domain), respectively.

For the DSMC method, the inflow nitrogen gas has a velocity $U_\infty = 1684.4835$ m/s with temperature $T_\infty = 273$ K, molecule number density $n = 1.2944 \times 10^{21}/\text{m}^3$, and the viscosity coefficient at upstream condition $\mu_\infty = 1.65788 \times 10^{-5}$ Ns/m^2. The cylinder has a cold surface with a constant temperature $T_w = 273$ K, with diffusive reflection boundary condition. The rotational collision number Z_r is defined in Eq. (28), where $\bar{T} = 91.5$ K and $(Z_r)_\infty = 18.1$.

For the UGKS method, the domain $(u, v) \in [-13.6, 13.6] \times [-13.6, 13.6]$ in velocity space is discretized with 93×93 mesh points based on Newton–Cotes rule, and the collision time is calculated with $\tau = \mu_\infty (T/T_\infty)^{0.78}/\text{P}$.

The comparison between UGKS and DSMC solutions are plotted in Figs. 10 and 11. In Fig. 10, the contour lines from DSMC and UGKS for density, velocity, total average temperature, translational temperature, and rotational temperature plotted together. Fig. 11 presents the flow variables along central symmetric line in front of the stagnation point, in which the density and U-velocity are matched very well, while for the temperature profiles, the temperature in UGKS solution upraise earlier than that in DSMC solution, and it is consistent with the solution of shock structure study [50].

5. Conclusions

In this paper, a unified gas-kinetic scheme has been developed for diatomic molecules in all flow regimes. The current UGKS is based on the Rykov equation with a Landau–Teller–Jeans-type relaxation model for the transitional and rotational energy exchange of a diatomic gas. The new scheme has been tested in a few cases, which include relaxation test of homogeneous flow, shock structure calculations, hypersonic rarefied flow passing through a flat plate, and the hypersonic flow around a blunt cylinder. The numerical results are compared with the analytic solutions, experimental measurements, and DSMC computations. Reasonable agreements between the UGKS results and other validated solutions have been obtained.

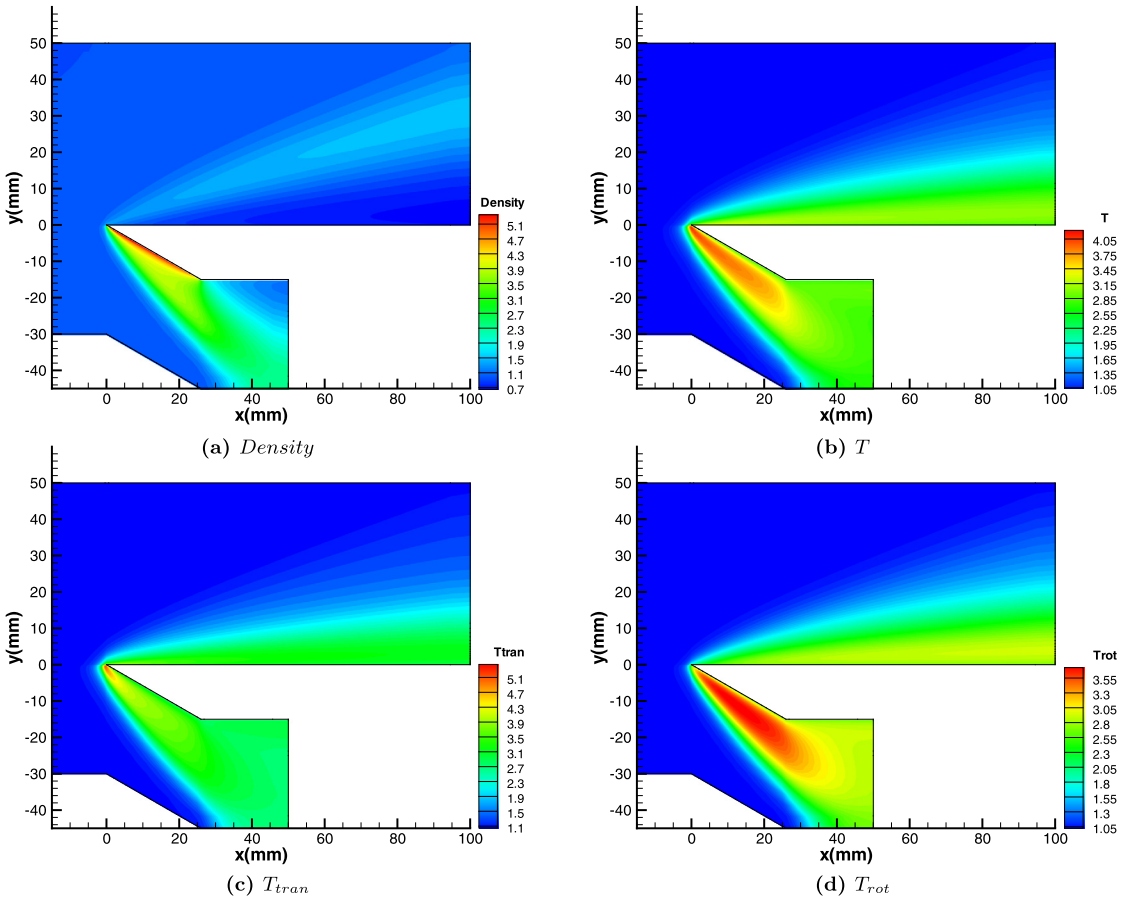

(a) *Density* (b) T

(c) T_{tran} (d) T_{rot}

Fig. 5. Macro-variable contours around the flat plate.

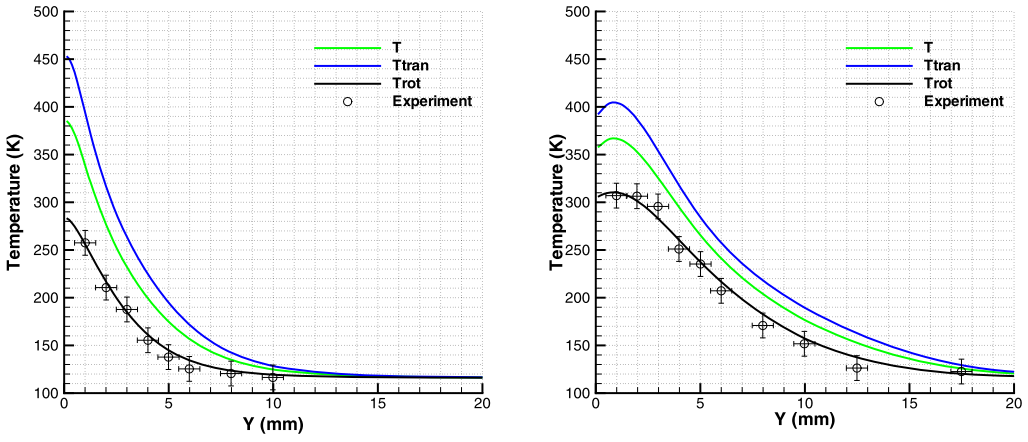

(a) *temperature plot at* $x = 5mm$ (b) *temperature plot at* $x = 20mm$

Fig. 6. Temperature plots along vertical lines at $x = 5$ mm and $x = 20$ mm.

Since local evolution solution of the Rykov model is used to construct a time-dependent gas distribution function around a cell interface, both kinetic and hydrodynamic scale flow physics has been included in the evolution. As a result, the distinguishable advantage of the UGKS is the applicability to simulate both continuum and rarefied flows. In the current UGKS, the numerical time step is determined by the CFL condition, which is not limited by the local particle collision time. At the same time, the mesh size is not limited by the mean free path. Through the extensive tests of the UGKS in the past

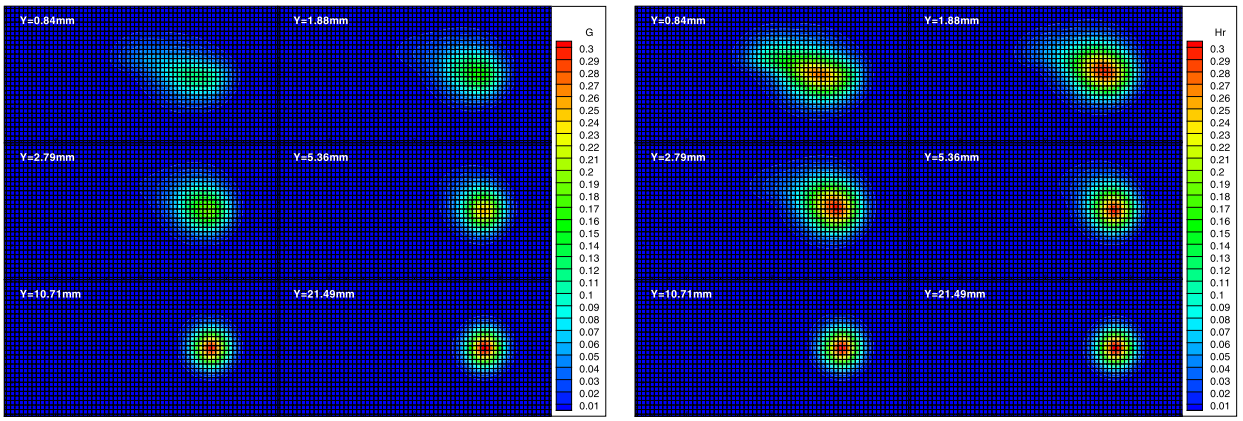

(a) *number distribution* G (b) *rotational energy distribution* R

Fig. 7. The distribution functions along vertical line at $x = 5$ mm.

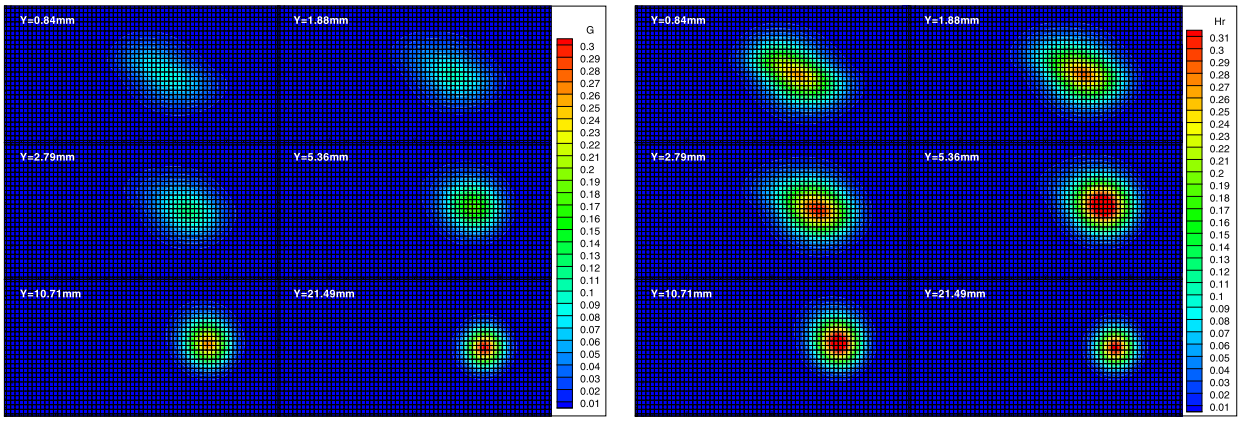

(a) *number distribution* G (b) *rotational energy distribution* R

Fig. 8. The distribution functions along vertical line at $x = 20$ mm.

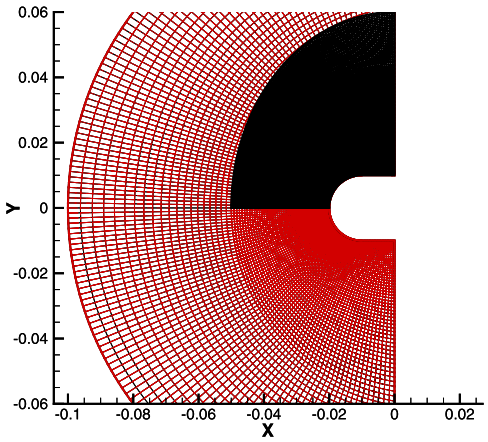

Fig. 9. Computational Meshes for UGKS and DSMC, black: DSMC, red: UGKS. (For interpretation of the references to color in this figure legend, the reader is referred to the web version of this article.)

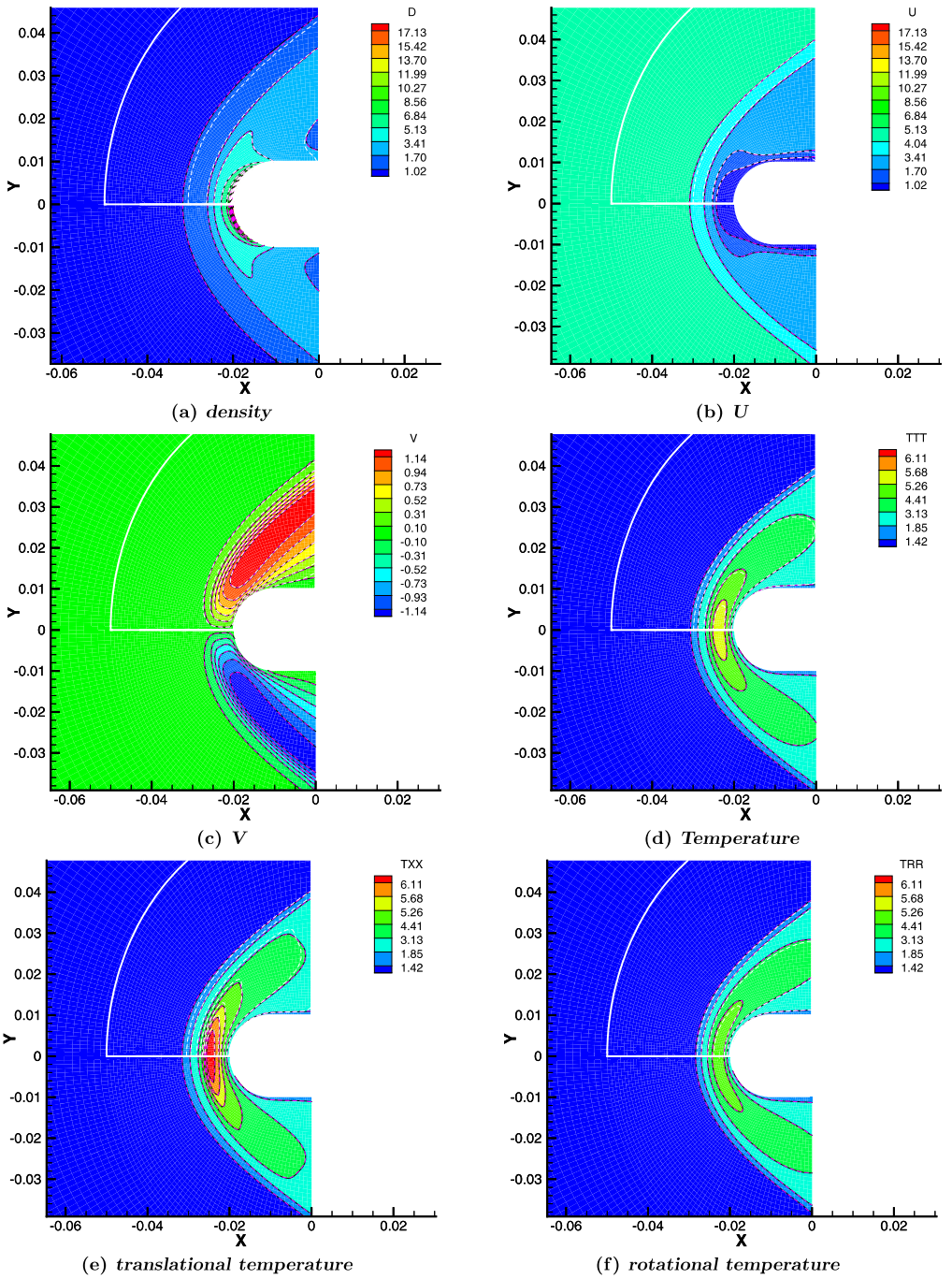

Fig. 10. Flow contours for nitrogen flows around a blunt cylinder at $Ma = 5.0$ and $Kn = 0.1$. White dashed lines: DSMC, background: UGKS.

years, now it is clearly demonstrated that the UGKS is a useful tool for the study of non-equilibrium flow, especially for the flow computations in the transition and near continuum regimes.

Acknowledgements

We would like to thank G.A. Bird and Q.H. Sun for helpful discussion and provide DSMC solutions. This work was supported by Hong Kong Research Grant Council (621011, 620813), grants SRFI11SC05 and FSGRF13SC21 at HKUST, and National High Technology Research and Development Program of China (Grant No. 2011AA7025042).

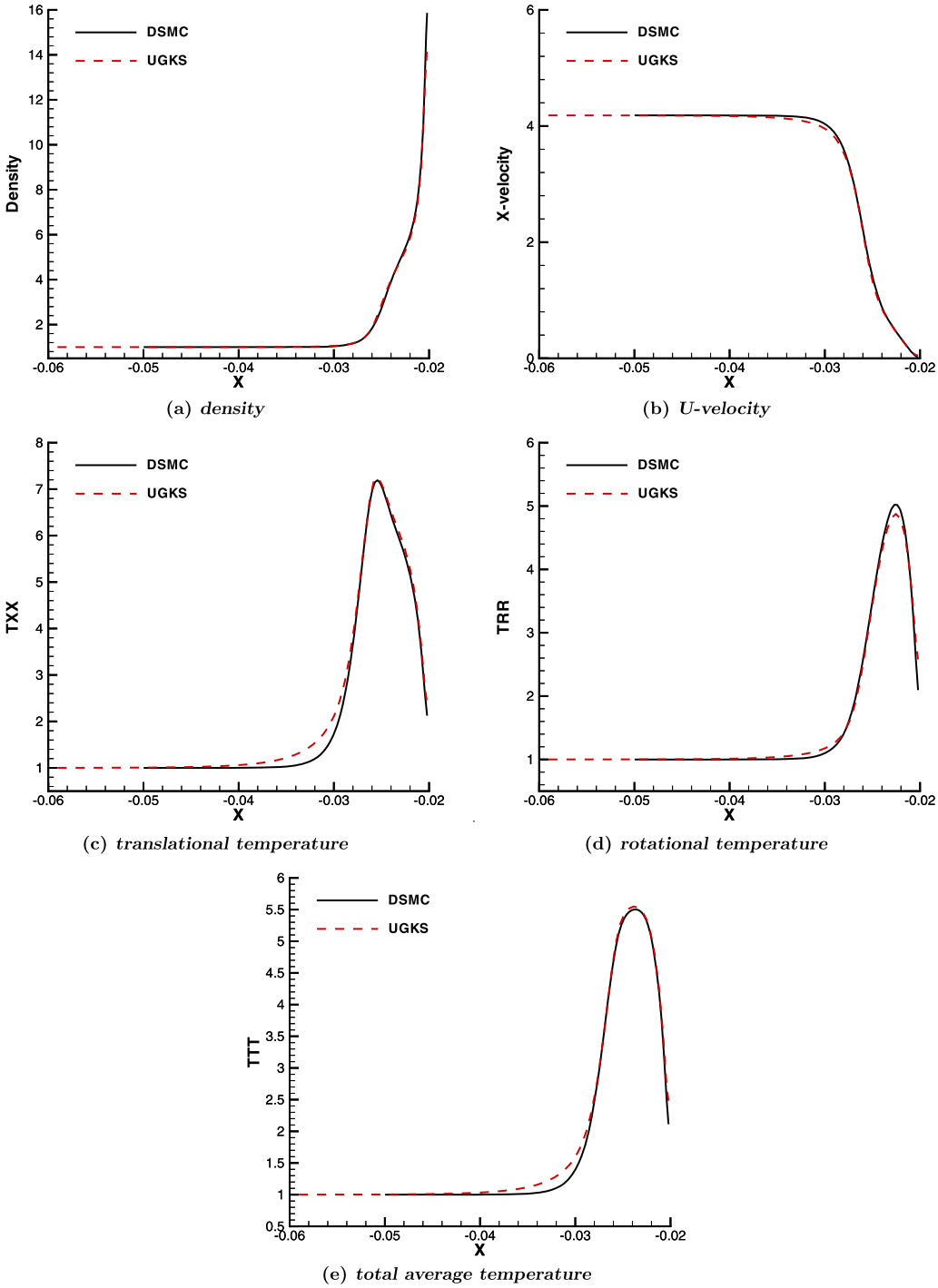

Fig. 11. Flow distributions for nitrogen gas along central symmetric line in front of the stagnation point at $Ma = 5.0$ and $Kn = 0.1$. Solid lines: DSMC, dashed lines: UGKS.

References

[1] G. Bird, Approach to translational equilibrium in a rigid sphere gas, Phys. Fluids 6 (10) (1963) 1518–1519.
[2] G. Bird, Monte Carlo simulation of gas flows, Annu. Rev. Fluid Mech. 10 (1) (1978) 11–31.
[3] G. Bird, Molecular Gas Dynamics and the Direct Simulation of Gas Flows, Clarendon Press, Oxford, 1994.
[4] V.V. Aristov, Direct Methods for Solving the Boltzmann Equation and Study of Nonequilibrium Flows, Kluwer Academic Publishers, Dordrecht, Netherlands, 2001.
[5] C. Chu, Kinetic theoretic description of the formation of a shock wave, Phys. Fluids 8 (1) (1965) 12–22.

[6] V. Kolobov, R. Arslanbekov, V. Aristov, A. Frolova, S. Zabelok, Unified solver for rarefied and continuum flows with adaptive mesh and algorithm refinement, J. Comput. Phys. 223 (2) (2007) 589–608.
[7] Z. Li, H. Zhang, Gas-kinetic numerical studies of three-dimensional complex flows on spacecraft re-entry, J. Comput. Phys. 228 (4) (2009) 1116–1138.
[8] J. Yang, J. Huang, Rarefied flow computations using nonlinear model Boltzmann equations, J. Comput. Phys. 120 (2) (1995) 323–339.
[9] L. Mieussens, Discrete-velocity models and numerical schemes for the Boltzmann–BGK equation in plane and axisymmetric geometries, J. Comput. Phys. 162 (2) (2000) 429–466.
[10] Y. Sone, T. Ohwada, K. Aoki, Temperature jump and Knudsen layer in a rarefied gas over a plane wall: Numerical analysis of the linearized Boltzmann equation for hard-sphere molecules, Phys. Fluids A 1 (2) (1989) 363–370.
[11] A.V. Bobylev, The theory of the nonlinear spatially uniform Boltzmann equation for maxwell molecules, Sov. Sci. Rev., C, Math. Phys. Rev. 7 (1988) 111–233.
[12] L. Wu, C. White, T.J. Scanlon, J.M. Reese, Y. Zhang, Deterministic numerical solutions of the Boltzmann equation using the fast spectral method, J. Comput. Phys. 250 (2013) 27–52.
[13] J. Meng, Y. Zhang, X. Shan, Multiscale lattice Boltzmann approach to modeling gas flows, Phys. Rev. E 83 (046701) (2011) 27–52.
[14] F. Filbet, S. Jin, A class of asymptotic-preserving schemes for kinetic equations and related problems with stiff sources, J. Comput. Phys. 229 (20) (2010) 7625–7648.
[15] S. Pieraccini, G. Puppo, Implicit–explicit schemes for BGK kinetic equations, J. Sci. Comput. 32 (1) (2007) 1–28.
[16] B. Dubroca, L. Mieussens, A conservative and entropic discrete-velocity model for rarefied polyatomic gases, in: ESAIM Proc., vol. 10, EDP Sciences, 2001, pp. 127–139.
[17] R. Agarwal, R. Chen, F. Cheremisin, Computation of hypersonic flow of a diatomic gas in rotational non-equilibrium past a blund body using the generalized Boltzmann equation, in: Parallel Computational Fluid Dynamics, Springer-Verlag, Berlin, Heidelberg, 2007, pp. 115–122.
[18] J. Wu, Z. Li, X. Jiang, One-dimensional shock-tube and two-dimensional plate flows in Boltzmann–Rykov model involving rotational energy, Chin. J. Comput. Phys. 30 (3) (2013) 326–336.
[19] L. Wu, Z.H. Li, X.Y. Jiang, One-dimensional shock-tube and two-dimensional plate flows in Boltzmann–Rykov model involving rotational energy, Chin. J. Comput. Phys. 30 (2013) 326–336.
[20] K. Xu, J. Huang, A unified gas-kinetic scheme for continuum and rarefied flows, J. Comput. Phys. 229 (20) (2010) 7747–7764.
[21] J. Huang, K. Xu, P. Yu, A unified gas-kinetic scheme for continuum and rarefied flows II: Multi-dimensional cases, Commun. Comput. Phys. 12 (3) (2012) 662–690.
[22] J. Huang, K. Xu, P. Yu, A unified gas-kinetic scheme for continuum and rarefied flows III: Microflow simulations, Commun. Comput. Phys. 14 (5) (2013) 1147–1173.
[23] S. Chen, K. Xu, C. Li, Q. Cai, A unified gas kinetic scheme with moving mesh and velocity space adaptation, J. Comput. Phys. 231 (20) (2012) 6643–6664.
[24] S. Liu, C. Zhong, Modified unified kinetic scheme for all flow regimes, Phys. Rev. E 85 (6) (2012) 066705.
[25] L. Mieussens, On the asymptotic preserving property of the unified gas kinetic scheme for the diffusion limit of linear kinetic models, J. Comput. Phys. 253 (2013) 138–156.
[26] S. Chen, K. Xu, A comparative study of an asymptotic preserving scheme and unified gas-kinetic scheme in continuum flow limit, arXiv:1307.4961 [physics.flu-dyn], 2013.
[27] Z. Guo, K. Xu, R. Wang, Discrete unified gas kinetic scheme for all Knudsen number flows: Low-speed isothermal case, Phys. Rev. E 88 (2013) 033305.
[28] K. Xu, A gas-kinetic BGK scheme for the Navier–Stokes equations and its connection with artificial dissipation and Godunov method, J. Comput. Phys. 171 (2001) 289–335.
[29] V. Rykov, A model kinetic equation for a gas with rotational degrees of freedom, Translated from Izv. Akad. Nauk SSSR, Meh. Židk. Gaza 1 (6) (1975) 107–115.
[30] P. Bhatnagar, E. Gross, M. Krook, A model for collision processes in gases. I. Small amplitude processes in charged and neutral one-component systems, Phys. Rev. 94 (3) (1954) 511–525.
[31] M. Kogan, Equations of motion of a rarefied gas, PMM 22 (4) (1958) 425–432.
[32] L. Holway, New statistical models in kinetic theory: methods of construction, Phys. Fluids 9 (9) (1966) 1658–1673.
[33] E. Shakhov, Generalization of the Krook kinetic relaxation equation, Izv. Akad. Nauk SSSR, Meh. Židk. Gaza 3 (5) (1968) 142–145.
[34] Y. Zheng, H. Struchtrup, Ellipsoidal statistical Bhatnagar–Gross–Krook model with velocity-dependent collision frequency, Phys. Fluids 17 (12) (2005) 127103.
[35] K. Xu, Regularization of the Chapman–Enskog expansion and its description of shock structure, Phys. Fluids 14 (4) (2002) L14–L20.
[36] K. Xu, L. Tang, Nonequilibrium Bhatnagar–Gross–Krook model for nitrogen shock structure, Phys. Fluids 16 (10) (2004) 3824–3827.
[37] K. Xu, E. Josyula, Continuum formulation for non-equilibrium shock structure calculation, Commun. Comput. Phys. 1 (3) (2006) 425–450.
[38] K. Xu, A generalized Bhatnagar–Gross–Krook model for nonequilibrium flows, Phys. Fluids 20 (2008) 026101.
[39] K. Xu, X. He, C. Cai, Multiple temperature kinetic model and gas-kinetic method for hypersonic nonequilibrium flow computations, J. Comput. Phys. 227 (14) (2008) 6779–6794.
[40] B. Van-Leer, Towards the ultimate conservative difference scheme V. A second order sequel to Godunov's method, J. Comput. Phys. 32 (1) (1979) 101–136.
[41] J. Parker, Rotational and vibrational relaxation in diatomic gases, Phys. Fluids 2 (4) (1959) 449–462.
[42] K. Koura, Statistical inelastic crosssection model for the Monte Carlo simulation of molecules with discrete internal energy, Phys. Fluids A 4 (8) (1992) 1782–1788.
[43] I. Boyd, Relaxation of discrete rotational energy distributions using a Monte Carlo method, Phys. Fluids A 5 (9) (1993) 2278–2286.
[44] M. Ivanov, S. Gimelshein, Computational hypersonic rarefied flows, Annu. Rev. Fluid Mech. 30 (1) (1998) 469–505.
[45] H. Alsmeyer, Density profiles in argon and nitrogen shock waves measured by the absorption of an electron beam, J. Fluid Mech. 74 (3) (1976) 497–513.
[46] N. Tsuboi, Y. Matsumoto, Experimental and numerical study of hypersonic rarefied gas flow over flat plates, AIAA J. 43 (6) (2005) 1243–1255.
[47] C. Cercignani, Rarefied Gas Dynamics, Cambridge University Press, 2000.
[48] G. Patterson, Molecular Flow of Gases, Wiley, New York, 1956.
[49] K. Xu, Z. Li, Microchannel flow in the slip regime: gas-kinetic BGK–Burnett solutions, J. Fluid Mech. 513 (1) (2004) 87–110.
[50] K. Xu, J. Huang, An improved unified gas-kinetic scheme and the study of shock structures, IMA J. Appl. Math. 76 (2011) 698–711.